

Strength, Deformation and Conductivity Coupling of Rock Joints

N. BARTON*
S. BANDIS†
K. BAKHTAR‡

Construction of dams, tunnels and slopes in jointed, water-bearing rock causes complex interactions between joint deformation and effective stress. Joint deformation can take the form of normal closure, opening, shear and dilation. The resulting changes of aperture can cause as much as three orders of magnitude change in conductivity at moderate compressive stress levels. Even the heavily stressed joints found in oil and gas reservoirs may also exhibit significant stress-dependent conductivity during depletion, and during waterflood treatments. The magnitudes of the above processes are often strongly dependent on both the character and frequency of jointing.

In this paper the results of many years of research on joint properties are synthesized in a coupled joint behaviour model. Methods of joint characterization are described for obtaining the necessary input data. The model simulates stress- and size-dependent coupling of shear stress, displacement, dilation and conductivity, and of normal stress, closure and conductivity. These processes are the fundamental building blocks of rock mass behaviour. Model simulations are compared with experimental behaviour and numerous examples are given.

INTRODUCTION

The strength and deformability of rock joints have been the subjects of numerous investigations, both for dam sites and for major rock slopes. Extensive reviews of such tests have been given by Link [1], Goodman [2], Cundall *et al.* [3], Bandis [4] and Barton and Bakhtar [5]. It has now been established beyond reasonable doubt that both the shear strength and deformability of rock joints are size-dependent parameters. See for example Pratt *et al.* [6], Barton and Choubey [7] and Bandis *et al.* [8]. The size dependence and general behaviour are governed to a large extent by surface characteristics such as roughness and wall strength, and by block size [9]. At the moderate stress levels of interest in civil engineering and in surface mining, differences in behaviour between rock types may therefore be marked. At very high stress levels, differences between rock types tend to be masked due to the extensive surface damage. See for example Barton [10] and Byerlee [11].

Basic elements of joint strength and deformability are summarized in Figs 1 and 2. In simplified terms, the stress-deformation behaviour of rock joints is convex-

shaped with shear loading [8], and concave-shaped with normal loading [12].

In a typical rock mass deformation test (i.e. a plate load test), the predominance of normal joint closure will usually result in concave load-deformation behaviour [13]. On occasions, such as in the NTS block test in Hanford basalt, [14], the shear components acting on hexagonal columnar jointing may be sufficiently strong to linearize the load-deformation behaviour. In effect, the convex and concave behaviours shown in Figs 1 and 2 are of roughly equal magnitude and cancel one another.

PART 1—CHARACTERIZATION

Joint Surface Characterization

Evidence that rock joint properties are dependent on surface characteristics such as roughness and wall strength can be deduced in part from the early work of Coulomb [15]. Direct physical evidence for the influence of surface joint properties were obtained by Jaeger [16], Patton [17], Rengers [18] and Barton [19]. Methods of quantifying roughness and wall strength and utilizing them in shear strength relations were developed by Barton and Choubey [7]. These methods were recently applied by Bandis [4] in his detailed studies of joint deformability and strength. As a result of this work it is now possible to predict shear strength-deformation behaviour and normal stress-closure behaviour with ac-

*Head—Dam, Rock and Avalanche Division, Norwegian Geotechnical Institute, P.O. Box 40, Tåsen, 0801 Oslo 8, Norway.

†Rock Engineer—1, Kalavriton Street, 551 33 Kalamaria, Thessaloniki, Greece. (1985 Research Fellow, NGI, Oslo, Norway.)

‡Manager—Applied Mechanics Group, Terra Tek Inc., 420 Wakara Way, Salt Lake City, UT 84108, U.S.A.

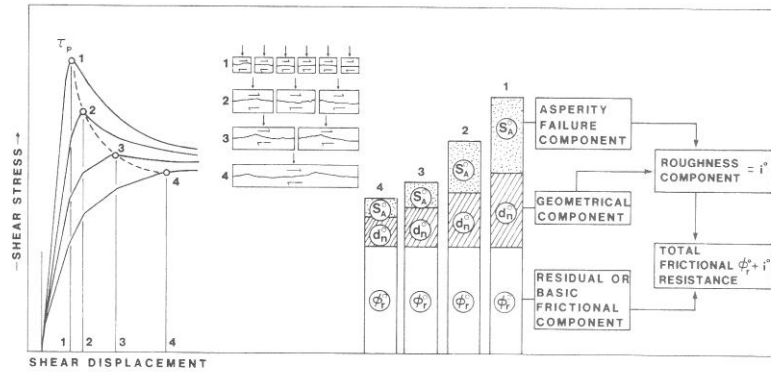


Fig. 1. An illustration of the size dependence of shear stress–deformation behaviour for non-planar joints. After Bandis *et al.* [8].

ceptable accuracy, using some very simple index tests to obtain the necessary input data. Since changes of joint aperture are also predictable, it is possible to couple joint conductivity with these stress changes.

The parameters required for complete joint characterization can be defined as follows:

- JRC—joint roughness coefficient;
- JCS—joint wall compression strength;
- σ_c —unconfined compression strength (rock adjacent to joint wall);
- ϕ_r —residual friction angle;
- e —conducting aperture;
- E —mechanical aperture.

Two of the parameters listed above can be obtained indirectly from extremely simple tilt tests using pieces of intact and jointed core, as shown in Fig. 3. The ideal

sample would be jointed axially, but routine testing can also include obliquely jointed samples, as typically recovered from a drilling program. The joint roughness coefficient (JRC) is obtained from such tests as follows:

$$JRC = \frac{\alpha - \phi_r}{\log(JCS/\sigma'_{no})} \quad (1)$$

where:

- α = tilt angle when sliding occurs;
- σ'_{no} = corresponding value of effective normal stress when sliding occurs (weigh upper sample, correct for $\cos \alpha$, measure joint area).

The value of JRC typically varies from zero to about 15, the former value corresponding to residual nondilatant joint surfaces for which $\alpha = \phi_r$.

The residual friction angle ϕ_r may be lower than the basic friction angle ϕ_b obtained from the tilt tests on core cylinders (lowest sketch Fig. 3) due to weathering or alteration effects. A simple empirical relation was devel-

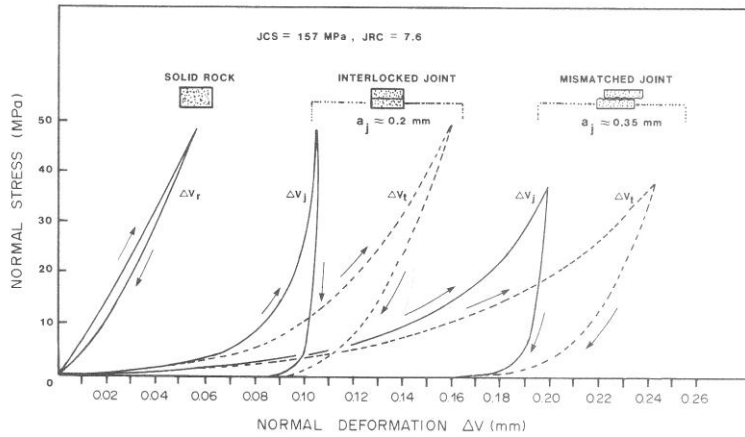


Fig. 2. Examples of normal stress–deformation behaviour for solid rock, and for an interlocked and mismatched joint. After Bandis *et al.* [12].

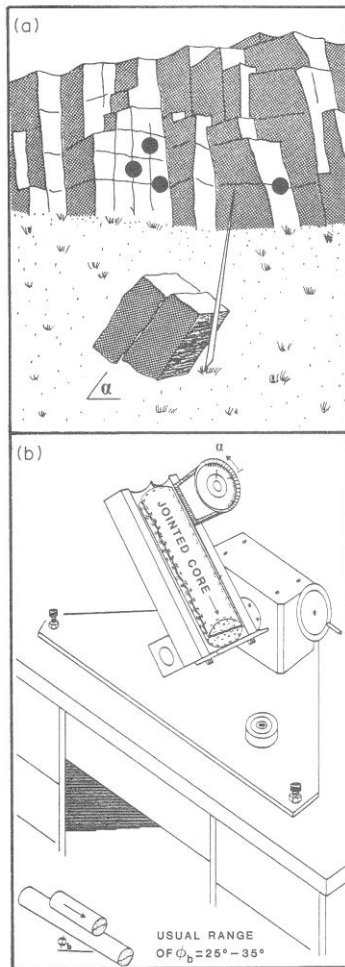


Fig. 3. Tilt tests for obtaining joint roughness and basic friction parameters.

oped by Barton and Choubey [7] to estimate ϕ_r from ϕ_b , using the Schmidt hammer. It is based on rebound tests on both the unweathered, dry rock (rebound R) and on the weathered and saturated joint wall (rebound r):

$$\phi_r = (\phi_b - 20) + 20r/R. \quad (2)$$

The Schmidt hammer test is also used to estimate the joint wall compression strength (JCS) of the fresh or altered joints in the saturated state, if this is appropriate to *in situ* conditions. The relationship derived by Miller [20] is used to convert the rock density and the rebounds (r) and (R) to estimates of the compression strengths JCS and σ_c , respectively. Full details of the above characterization tests were given by Barton and Choubey [7].

Example values of the above parameters might be as follows:

$$\begin{aligned} \alpha &= 66^\circ & \text{Equation (2) gives:} \\ \sigma'_{no} &= 0.001 \text{ MPa} & \phi_r = 26^\circ \text{ (moderately altered),} \\ r &= 40 \\ R &= 50 & \text{Equation (1) gives:} \\ \text{JCS} &= 100 \text{ MPa} & \text{JRC} = (66^\circ - 26^\circ)/5 = 8 \\ \phi_b &= 30^\circ & \text{(moderately rough).} \end{aligned}$$

Three of the above parameters (JRC, JCS, ϕ_r) are all that are needed to develop shear strength, displacement, dilation and normal stress-closure curves for any given joint. However, coupling conductivity with these processes requires additional information concerning the initial joint aperture, since closure or dilation resulting from stress changes are superimposed on these initial apertures.

Joint Aperture Characterization

There are several possible approaches for obtaining estimates of joint aperture. A direct approach used by Bandis [4] consisted of measuring aperture with a tapered feeler gauge, using plane sawn surfaces to gain access to the joints. The joints were interlocked, but under the very low normal stress generated by the self weight of the samples. Some 65 joint samples with varying degrees of weathering were measured in this way.

Barton and Bakhtar [5] derived the following empirical equation for estimating the initial mechanical aperture E_0 , based on the values of JRC and JCS recorded by Bandis [4]:

$$E_0 \approx \frac{\text{JRC}}{5} (0.2 \sigma_c / \text{JCS} - 0.1). \quad (3)$$

The relative alteration (σ_c / JCS) in this equation is a dimensionless number. The units of E_0 are millimetres. By implication, when a joint is unaltered or unweathered (i.e. $\text{JCS} = \sigma_c$), the initial aperture may be a function only of surface roughness.

A third approach for estimating aperture consists of indirect measurement using borehole pumping tests. Discrete joints are identified in borecore so that closely spaced straddle packers can be set to isolate individual features. The borehole flow test is interpreted in terms of the equivalent smooth wall (conducting) aperture given by:

$$e = (12k)^{0.5}, \quad (4)$$

where k is the conductivity in units of length squared.

Statistical interpretation of borehole pumping tests can also be used to obtain estimates of e , as described by Snow [21]. Numerous tests performed at US dam sites in the depth range 0–60 m indicated that most conducting apertures were in the range of 50–150 μm at this shallow depth. Borehole pumping tests performed across individual joints in crystalline rocks reported by Davison *et al.* [22], indicated a log-normal distribution of apertures over the depth range of 7–475 m, with a median value of only 25 μm .

On occasions when stress levels can be altered, using such methods as flat jack loading, conducting apertures

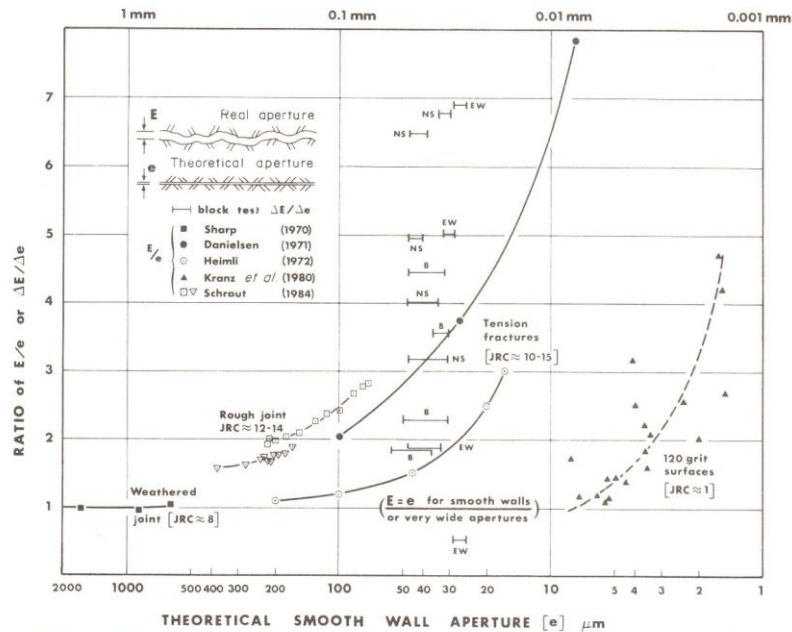


Fig. 4. Comparison of real mechanical apertures (E) with theoretical smooth wall conducting apertures (e). The mismatch is caused by flow losses due to tortuosity and surface roughness. After Barton [30].

can obviously be varied. For example, in an 8 m^3 block test performed by Hardin *et al.* [23] in jointed gneiss, the conducting aperture was reduced from 60 to $30 \mu\text{m}$ when the stress level was raised by 7 MPa. The 'undisturbed' conducting aperture (measured 1 m below the floor of the test tunnel) was $38 \mu\text{m}$ before the slots were drilled to insert the flat jacks. This increased to $60 \mu\text{m}$ due to the stress relief caused by slot drilling.

Modified Cubic Flow Law

Witherspoon *et al.* [24] suggested that the 'cubic law' relating flow rate to aperture cubed was valid for joints and fractures with apertures varying from $250 \mu\text{m}$ down to essentially closed features with apertures as small as $4 \mu\text{m}$. They implied that the real mechanical aperture was nearly the same as the conducting aperture, and that only slight reductions in flow rate (4–40%) could be attributed to roughness effects.

Analysis of the Witherspoon *et al.* [24] data reveals that the real mechanical apertures were never measured, since the samples were not instrumented prior to fracture formation. Estimates of the real mechanical apertures had to be obtained by adding measured changes of mechanical aperture to the calculated residual apertures—the conducting apertures remaining when the effective normal stress was as high as 20 MPa. Test data presented in Fig. 4 indicates that an erroneous estimate of mechanical aperture will be obtained by this method, due to the potentially large mismatch of e and E , when e is reduced by high stress levels.

The data shown in Fig. 4 were obtained from six sources and include flow tests in two tension fractures, between plane lapped (120 grit) surfaces and in three natural joints. The bars marked NS, EW and B represent large scale block test data from Hardin *et al.* [23] and indicate whether there was a shear stress component (NS or EW) or whether stresses were biaxial (B) resulting in pure normal stress across the test joint. Laboratory scale values of $JRC = 13$ and $JCS = 90 \text{ MPa}$ were measured on the rough mineralized joints intersecting this 8 m^3 block of gneiss.

The data presented in Fig. 4 can be approximated by an empirical equation incorporating a suitable term for roughness. For rock mechanics purposes, the roughness (JRC) obtained from a simple tilt test is obviously preferable to one obtained from asperity height statistics. The following equation provides an appropriate model of the data trends shown in Fig. 4.

$$e = JRC^{2.5} / (E/e)^3 \mu\text{m}. \quad (5)$$

Note that this equation is only valid for $E \geq e$. The units of e and E are microns.

The curves illustrated in Fig. 5 represent the predicted relation between E/e and conducting aperture. Plane, smooth surfaces with $JRC = 0$ will theoretically have conducting apertures exactly equal to mechanical apertures. This is consistent with observations of flow between optically plane glass plates. Furthermore, the model predicts that extremely rough surfaces will deviate from $E = e$ even at quite large apertures, an experimental detail that is also observed in practice.

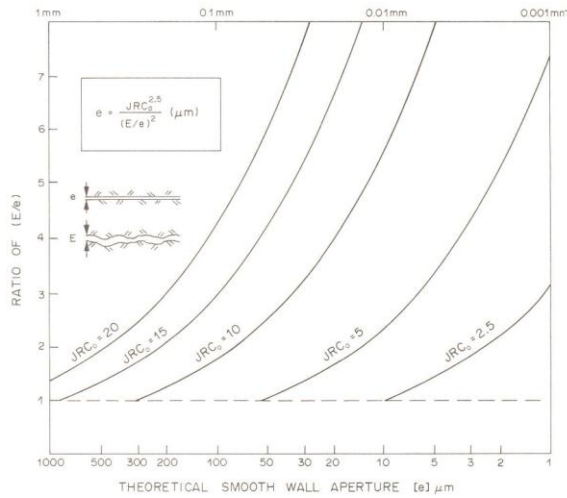


Fig. 5. An empirical relation incorporating joint roughness (JRC) and aperture which broadly satisfies the trends exhibited by available flow test data. After Barton [30].

PART II—CLOSURE

Normal Closure Behaviour

A detailed investigation of the normal closure behaviour of rock joints was recently published by Bandis [4] and Bandis *et al.* [12]. This incorporated multiple loading tests on 64 joint samples, representing five different rock types (slate, dolerite, limestone, siltstone and sandstone). As indicated in Fig. 2, this study included tests on interlocked joints, mismatched joints and intact samples representing similar grades of weathering. Deformation measured across the intact samples (ΔV_t) was subtracted from the total deformation measured across the jointed samples (ΔV_j) to obtain the net deformation of the joints (ΔV_j).

This method of correction means that the deformation characteristics of the weathered 'skin' on each side of the joints (if present) is incorporated in the results. This same skin of material influences the value of JCS obtained from Schmidt hammer tests, just as it may influence the value of JRC obtained (indirectly) from a tilt test. It is therefore not surprising that the relevant values of JCS and JRC can be used to predict normal closure behaviour, as shown by Bandis [4] and Bandis *et al.* [12].

An important aspect of the normal closure behaviour illustrated in Fig. 6 is the hysteresis and large permanent set seen in the first load cycle, when a 'disturbed' (unloaded) joint sample is first reloaded. *In situ* (undisturbed) samples probably react to stress change in a manner similar to the third or fourth cycle, when disturbances caused by sampling are largely removed.

Load history dependence was also exhibited by artificial tension fractures tested by Iwai [31] and in tests on natural joints and fractures reported by Gale [32]. Gale was one of the first to recognize the subtle differences between the stress–deformation and

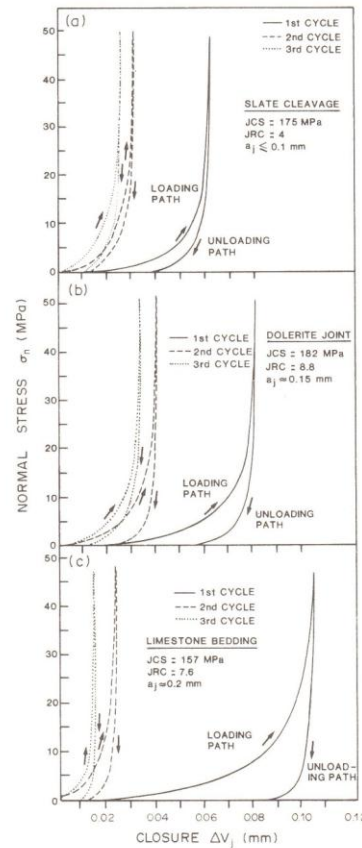


Fig. 6. Examples of normal closure cycles for three of the unweathered joints tested by Bandis [4].

stress–conductivity behaviour of artificial fractures and natural joints. It is especially important that tests on natural joints are used to develop stress–closure relations, since the extreme tightness and excessive roughness of artificial tension fractures produces a distorted behaviour relative to that of natural joints.

Normal Closure Modelling

The large body of experimental data produced by Bandis [4] has allowed improvements to be made in the earlier constitutive models for joint closure. The Bandis closure model incorporates hyperbolic loading and unloading curves, relating effective normal stress (σ_n) and joint closure (ΔV_j) as follows:

$$\sigma_n = \frac{\Delta V_j}{a - b \cdot \Delta V_j} \tag{6}$$

where a and b are constants. The initial normal stiffness (K_{ni}) is equal to the inverse of a , and the maximum possible closure (V_m) defines the asymptote a/b , as shown in Fig. 7. Empirical relations defining the magnitude of K_{ni} and V_m for each cycle of loading were derived from the experimental data. Details are given by Bandis *et al.* [12].

The extreme non-linearity of the stress–deformation behaviour seen in the stress range 0–20 MPa invalidates the use of constant normal stiffness values, as used in some finite element formulations. For each increment of σ_n the corresponding K_n value must be obtained from the derivative of the hyperbolic function (see Fig. 7). Interlocked joints with correlated upper and lower surfaces do not exhibit the proportionality between normal stress and stiffness that is seen in mismatched (uncorrelated) surfaces.

A detailed description of the numerical methods needed to model three or four load–unload cycles for any given rock joint is beyond the scope of this paper. Important source material will be found in Bandis [4] and Bandis *et al.* [12]. Model development is described by Barton [30] and Barton and Bakhtar [5].

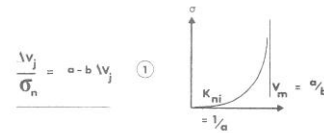
Figure 8 illustrates four examples of stress–closure modelling. The only input parameters required for this stage of modelling are the roughness (JRC), the wall strength (JCS) and the initial mechanical aperture (E_0). The latter has been derived from equation (3) in these four examples, hence the use of σ_c values.

The subscripts JCS₀ and JRC₀ indicate the use of laboratory scale parameters for normal closure modelling. Scale effects are assumed to be of only minor consequence to normal closure due to the dominant effect of the small scale roughness. The most likely effect of scale on closure will be due to sampling disturbance. It is easier to ensure perfect fit with small samples than large samples. In the undisturbed state, this problem does not arise. However, when shearing occurs, scale effects may prove of extreme importance since the small scale roughness ceases to be in intimate contact.

The four examples shown in Fig. 8 are presented in pairs. In examples A and B the relative alteration (150/100) is held constant, and JRC is given values of 5

NORMAL CLOSURE OF JOINTS

(HYPERBOLIC FUNCTION)



$$V_m \approx A + B [JRC_c] + c \left[\frac{JCS_c}{\sigma_j} \right]^D \tag{2}$$

$$K_{ni} \approx 0.02 \left[\frac{JCS_c}{\sigma_j} \right] + 2 JRC_c - 10 \tag{3}$$

NORMAL STIFFNESS OF JOINTS

(derivative of hyperbolic function)

$$K_n = K_{ni} \left[1 - \frac{\sigma_n}{V_m K_{ni} + \sigma_n} \right]^{-2}$$

I. INTERLOCKING JOINTS

i.e. K_n is not proportional to σ_n



II. MISMATCHED JOINTS

K_n is proportional to σ_n



Fig. 7. The constitutive model for joint closure developed by Bandis [4].

(moderately smooth) and 15 (rough, undulating). Initial mechanical apertures are estimated as 200 and 600 μ m from equation (3). It is readily observed that closure under load is more complete in the smooth joint than in the rough joint. The steepness of asperities in a rough undulating joint inhibits closure due to the marked shear components. This behaviour is consistent with experimental observations reported by Bandis *et al.* [12], Schrauf [29] and others.

In the second pair of examples shown in Fig. 8 (C and D), joint roughness (JRC) is held constant at 10 (moderately rough) while the relative alteration is increased from 1.33 to 3.0. Model results are again consistent with experience. The stress–closure cycles stabilize more rapidly in the less altered joint, while continued closure is evident in the more highly altered joint. In general the residual apertures remaining after four consolidation cycles tend to be least for smooth-planar-unaltered joints and most for rough-undulating-altered joints. Detailed

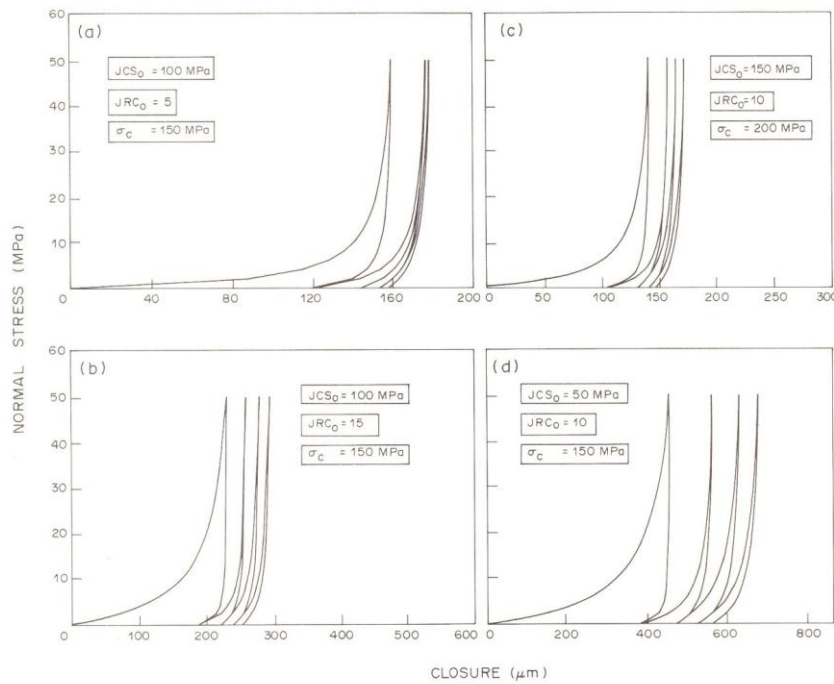


Fig. 8. Stress closure modelling, showing the influence of roughness and alteration. After Barton and Bakhtar [5].

comparisons of modelled and measured joint closure cycles are given by Barton and Bakhtar [5].

Closure-Conductivity Coupling

The above model describing changes of mechanical aperture (ΔE) with normal stress, provides simultaneous data concerning the residual mechanical aperture (E) by subtraction from the initial aperture E_0 :

$$E = E_0 - \Delta E. \tag{7}$$

Equations (4), (5) and (7) can be used to estimate joint conductivity, based on conversion from the residual mechanical apertures (E) to the residual conducting apertures (e), the conductivity being proportional to e^2 .

Figure 9 shows an example of this stress-closure-conductivity modelling. On the fourth cycle of loading which is assumed to return the joint to undisturbed (*in situ*) levels of consolidation, the residual mechanical aperture of approximately 200 μm converts to a conductivity of approximately 10^{-5} cm^2 (1000 darcies). The change of gradient seen in cycle 1 (marked with large arrow) represents the transition from $e = E$ to $e < E$, according to the empirical relationship represented in Fig. 5. As the joint is closed further by successive load cycles divergence from $e = E$ increases, resulting in successively steeper conductivity-stress gradients. The open and closed circles marked on the fourth load cycle are utilized later as initial conditions for shear-dilation-conductivity coupling.

Comparison with measured data

A recent application of the foregoing methods of joint characterization and closure-conductivity modelling will

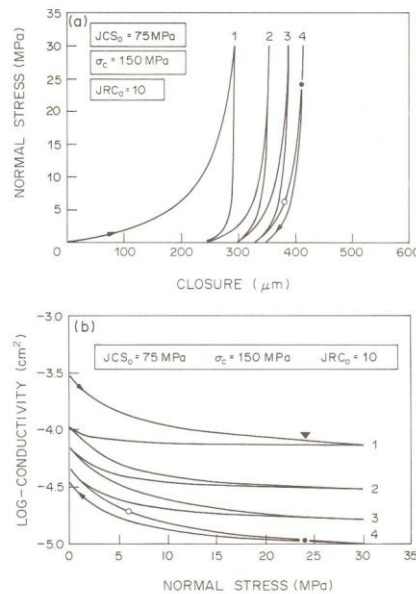


Fig. 9. Stress-closure-conductivity coupling for a moderately altered, medium rough joint.

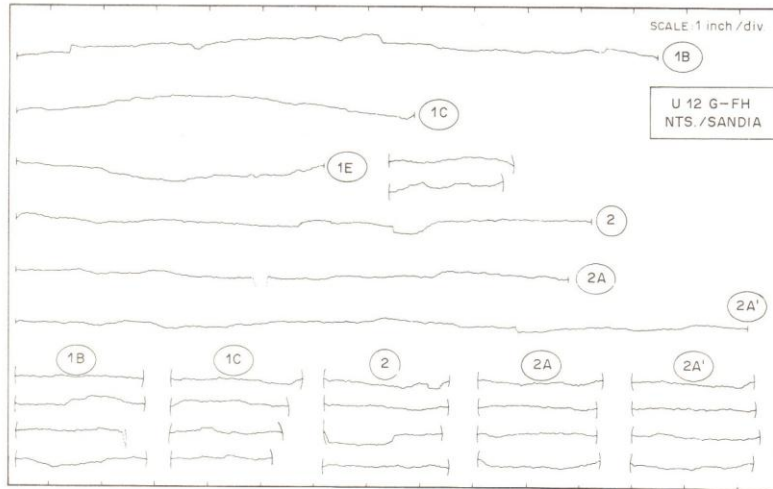


Fig. 10. Roughness profiles of jointed core from Sandia National Laboratories No. 1 small diameter heater alcove, at the Nevada Test Site. Axial and diametral profiles are shown.

now be given, to illustrate the potential of the technique. The work was performed on jointed samples of welded tuff from G-tunnel in the Nevada Test Site. Sandia National Laboratories provided six axially jointed samples from their No. 1 small diameter heater alcove. Axial and diametral roughness profiles for these joints are reproduced in Fig. 10.

Tilt tests were performed on the samples in the manner illustrated in Fig. 3 (lower diagram). The average tilt angle (α°) obtained from these tests was 71.4° and the average value of ϕ_b was 29.5° .

Seventy two Schmidt hammer tests were performed on exposed joint surfaces in the underground test facility. The mean rebound value of 45 and the rock density of 2.3 g/cm^3 convert to an estimated 82.5 MPa for the joint wall compression strength, according to the well known relation derived by Miller [20].

The following laboratory scale values of input data were used in subsequent modelling of these joints:

$$\begin{aligned} JRC_0 &= 9.0, & JCS_0 &= 82.5 \text{ MPa}, \\ \phi_r = \phi_b &= 29.5^\circ \text{ (unweathered)}. \end{aligned}$$

These data were sufficient to generate shear stress–displacement–dilation and normal stress–closure curves, but an estimate of initial aperture was required to couple conductivities to these mechanical changes. Since jointed samples were available it was possible to measure the initial aperture without resorting to approximation using equation (3).

The approach adopted was to set the largest available sample (profile 2A', Fig. 10) in a rubber sleeve and conduct a flow test using a constant-head water supply. An initial conducting aperture (e_0) of $401 \mu\text{m}$ was calculated from these tests, under an effective stress of zero (nominal). This aperture was used as the initial condition when modelling stress–closure–conductivity coupling. The resulting model is shown in Fig. 11.

The fourth load cycle is presumed to approximate undisturbed *in situ* conditions. The mechanical and conducting apertures predicted for three levels of effective normal stress (10, 20 and 30 MPa) are listed in the figure to demonstrate the relative magnitudes of e and E under consolidated conditions.

A large scale flat-jack loaded block test performed on joints in welded tuff in the same underground test facility, indicated conducting apertures in the range $68\text{--}57 \mu\text{m}$ under ambient temperature, biaxial (normal)

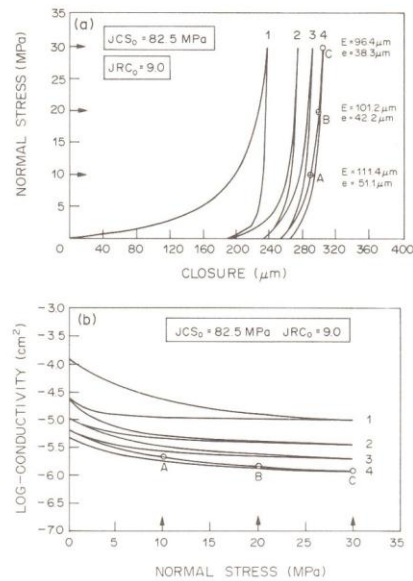


Fig. 11. Example of stress–closure–conductivity modelling for joints in welded tuff obtained from Sandia National Laboratories G-tunnel test facility at the Nevada Test Site.

Table 1. Predicted mechanical and conducting apertures

σ'_n (MPa)	E (μm)	e (μm)
0	148.6	90.9
2	135.0	75.0
4	126.0	65.4
6	119.7	59.0

These conducting apertures are within some few percent of the values actually measured over the stress range 1–5 MPa.

loading, over a stress range of approximately 1–5 MPa. Our model results for fourth cycle loading are shown in Table 1.

Application of the above methods to petroleum reservoir technology appear warranted if this level of prediction is repeatable. The marked changes of conductivity seen when the effective normal stress increases from say 5 to 15 MPa, provides an explanation for reduced production with reservoir life. Reversal of this trend by waterflooding is also explained and may be predictable.

PART III—SHEAR

The four type curves illustrated in Fig. 1 indicate that shear stress–displacement behaviour can range from the classic peak-residual bi-linear curves to quite smooth hyperbolic curves. The peak-residual behaviour is most typical for small block sizes, rough joints, and low ratios of σ'_n/JCS . The smooth hyperbolic behaviour results from exactly opposite characteristics: i.e. large block sizes, smooth joints and high ratios of σ'_n/JCS .

Considering only pre-peak behaviour, it is apparent that hyperbolic relations of the type proposed by Kuhlhawy [33] or Hungr and Coates [34] could be used to formulate behaviour. However, post-peak behaviour, which may often incorporate negative slopes as residual strength is approached, requires a more comprehensive treatment.

Mobilization of Roughness During Shear

The joint roughness coefficient JRC introduced earlier, specifically related to peak shear strength. The corresponding peak drained friction angle (ϕ') can be expressed as follows:

$$\phi' = \text{JRC} \cdot \log(\text{JCS}/\sigma'_n) + \phi_r \quad (8)$$

This peak strength is mobilized following a small shear displacement denoted by δ (peak). A review by Barton and Bandis [9] indicated that δ (peak) is frequently about 1% of the joint sample length (L) for the case of laboratory-size samples (nominally $L_0 = 100$ mm for laboratory samples). During this first 1 mm of shear displacement ϕ_r is mobilized first, and then roughness, causing dilation. Post-peak, at displacements larger than our example 1 mm, roughness is gradually destroyed or worn down. Dilation continues but at a reduced rate post-peak.

It is obviously convenient to formulate the general case in which the strength at any given shear displace-

ment (δ) is denoted by ϕ (mobilized), whose value depends on the corresponding magnitude of JRC (mobilized):

$$\phi'(\text{mob}) = \text{JRC}(\text{mob}) \cdot \log(\text{JCS}/\sigma'_n) + \phi_r \quad (9)$$

It has recently been established by Barton [30] that the dimensionless co-ordinates $\text{JRC}(\text{mob})/\text{JRC}(\text{peak})$ and $\delta/\delta(\text{peak})$ increase during shear in an almost identical manner for a wide variety of joint surfaces and for a wide range of stress levels. We can therefore utilize a standard table of values for these dimensionless terms to predict shear stress–displacement behaviour for joints having any desired values of JCS, JRC and ϕ_r . This can be done for any stress level of interest.

An example of this new formulation of shear stress–displacement behaviour is illustrated in Fig. 12. The following key aspects of behaviour are modelled in the order in which they occur during a shearing event.

- (1) Friction is mobilized when shearing begins.
- (2) Dilation begins when roughness is mobilized.
- (3) Peak strength is reached at $\text{JRC}(\text{mob})/\text{JRC}(\text{peak}) = 1.0$, $\delta/\delta(\text{peak}) = 1.0$.
- (4) Dilation declines as roughness reduces.
- (5) Residual strength is finally reached.

Equations (8) and (9) provide the required values of $\text{JRC}(\text{mob})/\text{JRC}(\text{peak})$ from initiation, through peak strength and down to residual strength. It is readily shown that:

$$\frac{\text{JRC}(\text{mob})}{\text{JRC}(\text{peak})} = \frac{\phi'(\text{mob}) - \phi_r}{\phi'(\text{peak}) - \phi_r} \quad (10)$$

At the initiation point, $\phi'(\text{mob})$ is zero and the co-ordinates are therefore given by:

$$1. \frac{\text{JRC}(\text{mob})}{\text{JRC}(\text{peak})} = -\frac{\phi_r}{i}$$

where

$$i = \text{JRC}(\text{peak}) \cdot \log(\text{JCS}/\sigma'_n).$$

$$2. \frac{\delta}{\delta(\text{peak})} = 0.$$

An empirical equation for $\delta(\text{peak})$ developed by Barton and Bandis [9] from analysis of 650 shear test data, provides an estimate of $\delta(\text{peak})$ that is dependent on the sample length (L_n) and the roughness JRC_n of this length of sample. (See subsequent discussion of scale effects.)

In the following equation $\delta(\text{peak})$ and L_n are both given in metres.

$$\delta(\text{peak}) = \frac{L_n}{500} \left[\frac{\text{JRC}_n}{L_n} \right]^{0.33} \quad (11)$$

The fundamental shape of the dimensionless shear stress–displacement model illustrated in Fig. 12 depends on the character of the joint (JCS, JRC and ϕ_r) and on the level of effective normal stress. In the example shown we have chosen the following values:

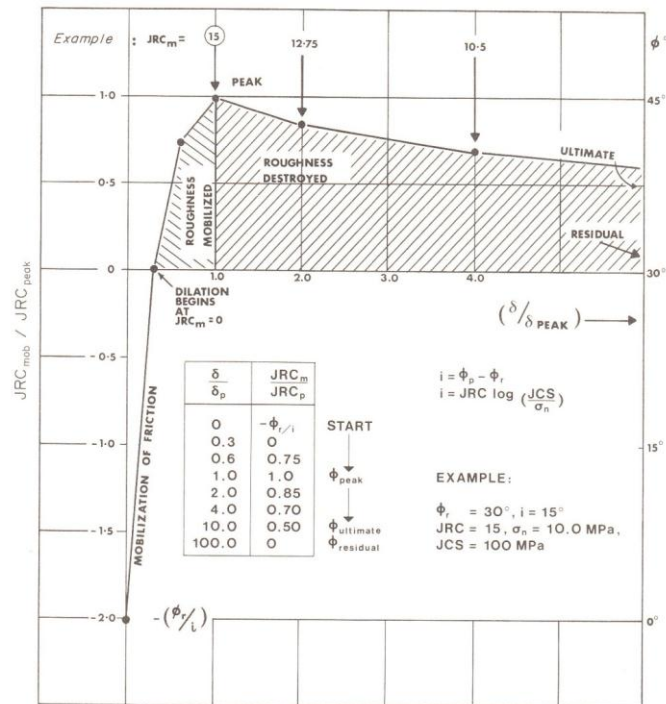


Fig. 12. Dimensionless model for shear stress-displacement modelling, after Sharp [25]. In this example $\phi_p/i = 2$.

$$JCS = 100 \text{ MPa};$$

$$JRC = 10;$$

$$\sigma'_n = 10 \text{ MPa};$$

$$\phi_r = 30^\circ.$$

These input parameters give a peak i value of 15° , and therefore $-(\phi_r/i)$ is equal to -2.0 in this example.

The simplified table of values given as an inset in Fig. 12 give the principal co-ordinates necessary to define a complete shear stress-displacement event. The curves generated can range from sharply peaked to smooth and rounded. Note that reversed shear can also be handled using these techniques [30].

Comparison with measured data

There are numerous sets of shear stress-displacement data available in the literature. At present, their chief drawback as a source of validation for constitutive models is that the relevant joints are not fully characterized. Roughness will typically be described verbally, but there are seldom enough data to allow quantification of either roughness or the strength of the rock. Since each sample is unique, attempts at parametric studies are usually dominated by sample variation.

A solution to this lack of useable data is the use of cast replicas of rock joints, formed with brittle rock simulants. This allows identical samples to be reproduced at

will, so that an experimental variable such as normal stress level can be investigated, without the complication of variation in other properties. Furthermore, the use of cast replicas allows repeated tests to be performed using samples of different size.

Bandis [4] and Bandis *et al.* [8] described a comprehensive series of shear test data using numerous cast replicas of eleven different joints. In all the shear tests performed, detailed information concerning JRC, JCS and ϕ_r was available.

Figure 13 shows examples of the shear stress-displacement data obtained from physical replicas of joints. In the upper left hand diagram, three tests conducted on identical joint replicas at three normal stress levels are compared with the numerical model (top right diagram). In the lower pair of diagrams, four tests run at equal stress levels on four joints of different roughness are compared. Excellent agreement between the model and the physical data is indicated.

Size Effects

The extensive size effects investigation performed by Bandis [4], and earlier work by Pratt *et al.* [6] and Barton and Choubey [7] revealed an important size effect on joint shear behaviour. The shear stiffness is the parameter affected most, due to simultaneous reductions in strength and increases in peak displacement as joint dimensions (specifically length L) are increased.

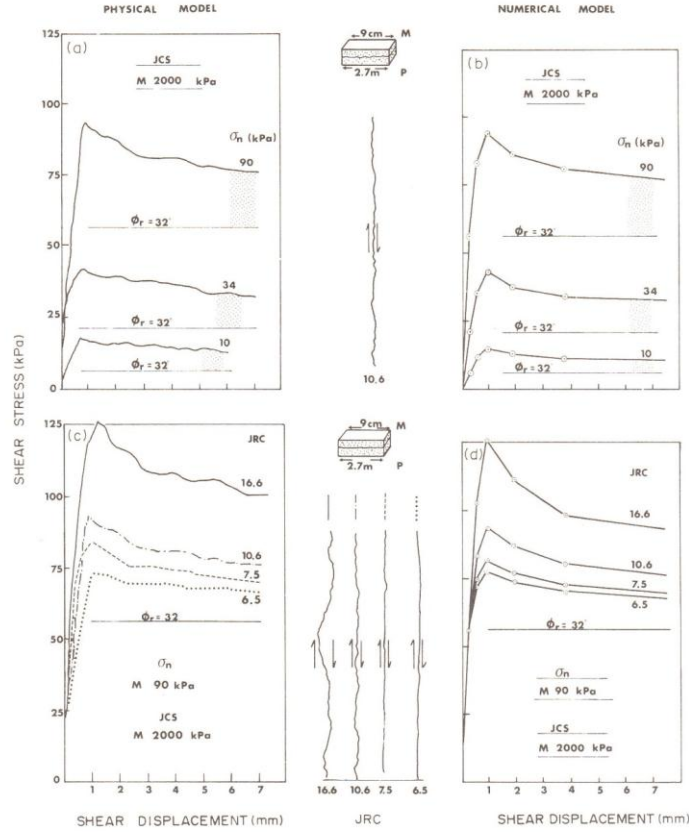


Fig. 13. Comparison of shear stress–displacement data obtained from numerical models and physical models.

A review of some 650 data points from 35 sources by Barton and Bakhtar [5] which is shown in Fig. 14, reveals the strong influence of block size and stress level. Note that the dotted lines representing constant stress level are estimates of the experimental trends observed in the size range 100–1000 mm.

In the context of the present joint modelling, increased joint size causes marked reductions in JRC and JCS and increases in δ (peak). The magnitude of expected size effects depends on the value of JRC_0 , the laboratory scale roughness, as shown by Bandis *et al.* [8]. Formulations for these size effects were developed by Barton and Bandis [9] and are reproduced below. The nomenclature adopted incorporates the subscripts (0) and (n) for laboratory scale and *in situ* scale values respectively:

$$JRC_n = JRC_0 \left[\frac{L_n}{L_0} \right]^{-0.02JRC_0} \quad (12)$$

$$JCS_n = JCS_0 \left[\frac{L_n}{L_0} \right]^{-0.03JRC_0} \quad (13)$$

Examples of the shear stiffness scale effects predicted by equations (11), (12) and (13) are illustrated in Fig. 15.

A rough, high strength joint and a smoother weathered joint are assumed as laboratory scale input. It will be noted that the shear stiffnesses of the two joint types converge to similar values as either the stress level or the size of sample is increased.

A convenient property of the dimensionless shear stress–displacement model shown in Fig. 12 is that the above equations giving the large scale values of JRC_n and δ_n (peak) can be applied directly to give the appropriate full-scale dimensionless co-ordinates:

$$\frac{JRC_n(\text{mob})}{JRC_n(\text{peak})} \quad \text{and} \quad \frac{\delta_n}{\delta_n(\text{peak})}$$

The scaling relations provide successively lower values of JRC_n (peak) and larger values of δ_n (peak) as sample size increases. The co-ordinates listed in Fig. 12 take care of the complete curve modelling process, at any desired scale.

It should be noted that the joint length L_n used to represent *in situ* block size is assumed to be equal to the average spacing of the joints that intersect the joints in question. These cross-joints act as potential ‘hinges’ in

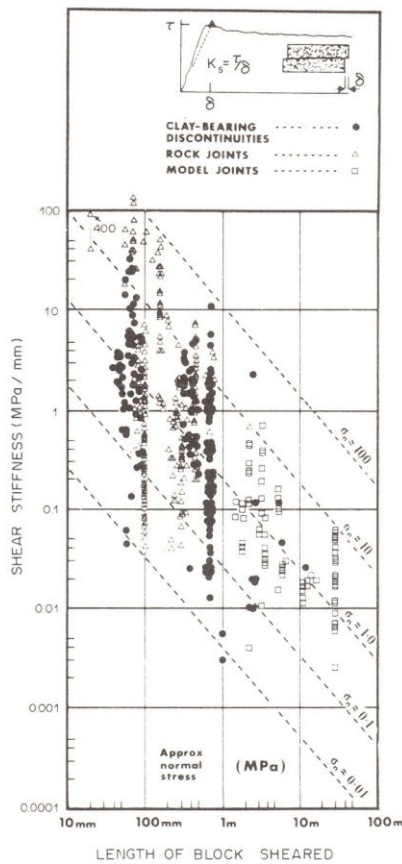


Fig. 14. Summary of 650 test data showing the scale and stress dependency of peak shear stiffness for a variety of discontinuity types. After Barton and Bakhtar [5].

the rock mass, and limit the size effect to this maximum dimension of joint surface, according to multiple block shear tests reported by Barton and Bandis [9]. An exception to the above assumption would be the case of a joint set that is gently folded. Major undulations would never be sheared and would obviously extend the scale effect to a larger joint dimension. Such undulations could be allowed for by adding a constant angle i to the residual friction angle ϕ_r in equations (8) and (9).

Comparison with measured data

Figure 16 illustrates the average shear stress–displacement data from one of the size effect investigations performed by Bandis [4]. Eighteen samples measuring 60 mm in length, nine measuring 120 mm, four measuring 180 mm and one measuring the full 360 mm were tested in various sizes of shear box. Each of these particular samples was a portion of identical cast replicas of a bedding plane in limestone, whose roughness profile is also shown in the figure.

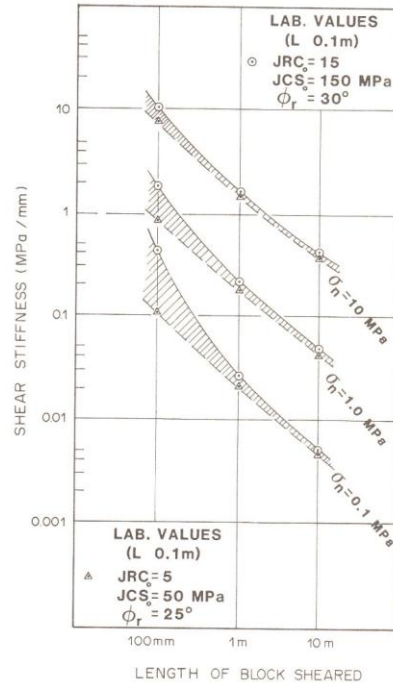


Fig. 15. Shear stiffness scale effects predicted by the empirical equations relating δ (peak), JRC_n and JCS_n to sample size (L_n).

Our numerical model was used to generate corresponding sets of shear stress–displacement curves, using the following input data obtained from the smallest physical models:

$$JRC_0 = 15.0, \quad JCS_0 = 2 \text{ MPa}, \quad \phi_r = 32^\circ.$$

The normal stress applied in both the physical and numerical model was 24.5 kPa. At prototype scale (40:1) the stress/strength ratio represented was 2 MPa/80 MPa. The comparison of physical and numerical data is seen to be excellent. All of the characteristic size effects illustrated in Fig. 1 appear to be modelled in a realistic manner.

Dilation Modelling

When shearing of a non-planar joint occurs, the opposed asperities slide over each other and cause an increase in aperture. This dilation process requires a finite displacement to get started, and occurs at an increasing rate as peak strength is approached. The maximum angle of dilation occurs coincidentally with the mobilization of peak shear strength and can be estimated from the following equation [7]:

$$d^{\circ}(\text{peak}) = 1/2 JRC(\text{peak}) \cdot \log(JCS/\sigma'_n). \quad (14)$$

It is found that this peak dilation angle can be generalized in a similar manner to $\phi'(\text{peak})$ to account for pre-peak and post-peak shearing [30]. Thus:

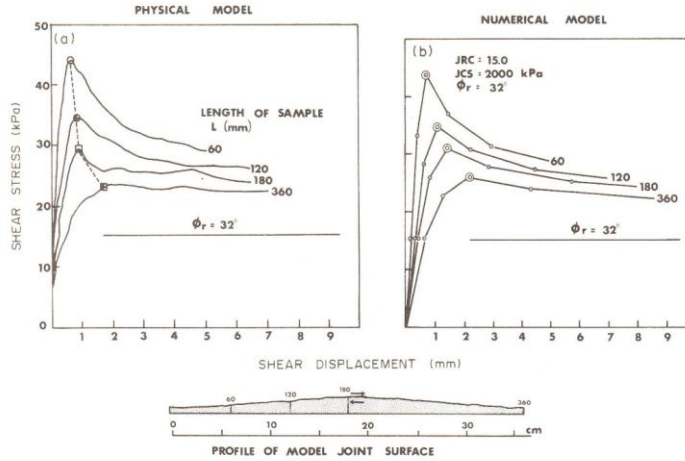


Fig. 16. Modelling the shear stress-displacement data obtained from physical joint replicas of various sizes. Physical data was obtained from Bandis [4].

$$d_n^o(\text{mob}) = 1/2 JRC(\text{mob}) \cdot \log(JCS/\sigma'_n) \quad (15)$$

Experience has shown that the subscript n can be added to parameters in both these equations, to provide for the large scale behaviour of samples of length L_n . Thus, equation (15) can be generalized to represent any sample size:

$$d_n^o(\text{mob}) = 1/2 JRC_n(\text{mob}) \cdot \log(JCS_n/\sigma'_n) \quad (16)$$

An important aspect of dilation behaviour identified by Bandis *et al.* [8] is that dilation initiates at larger shear displacements as sample length increases. The stress-displacement model illustrated in Fig. 12 shows dilation initiating when $\delta/\delta(\text{peak})$ is equal to 0.3. Since $\delta_n(\text{peak})$ increases with sample size following equation (11), dilation will also be initiated with due respect for sample size.

Figure 17 illustrates the scaling potential of the model up to this stage of development. It is assumed that a 100 mm long laboratory sample is the only source of data available, and is characterized as follows:

$$JRC_0 = 15, \quad JCS_0 = 150 \text{ MPa}, \quad \phi_r = 30^\circ.$$

Scaling equations (11), (12) and (13) provide appropriate values of JRC_n , JCS_n and $\delta_n(\text{peak})$ for sample sizes of 1 and 2 m, as shown in the inset to the figure. Corresponding shear stress-displacement and dilation-displacement curves are shown. The potentially misleading nature of laboratory-scale shear tests in the case of strong, rough joints is clearly illustrated. Note the 'delayed' initiation of dilation in the lower diagram, and the location of the peak dilation angles (double circles) which correspond to the peak strength locations in the upper diagram.

Comparison with measured data

Figure 18 illustrates the average dilation-displacement data from one of the size effects investigations performed

by Bandis [4]. Eighteen samples measuring 60 mm in length, nine measuring 120 mm, four measuring 180 mm and one measuring the full 360 mm were tested in

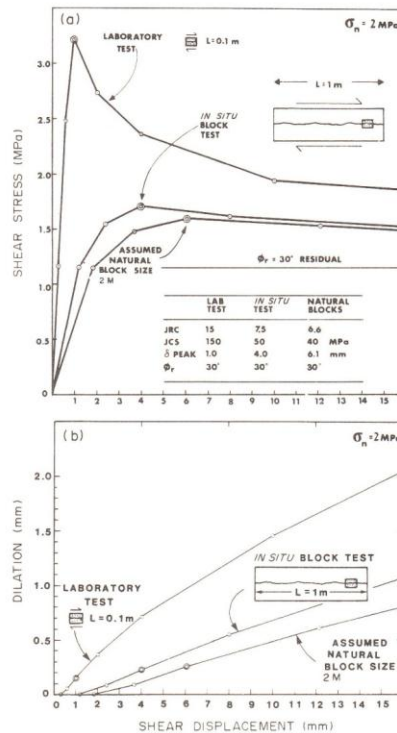


Fig. 17. Modelling the shear stress-displacement and dilation-displacement behaviour of different block sizes, assuming a constant effective normal stress of 2 MPa.

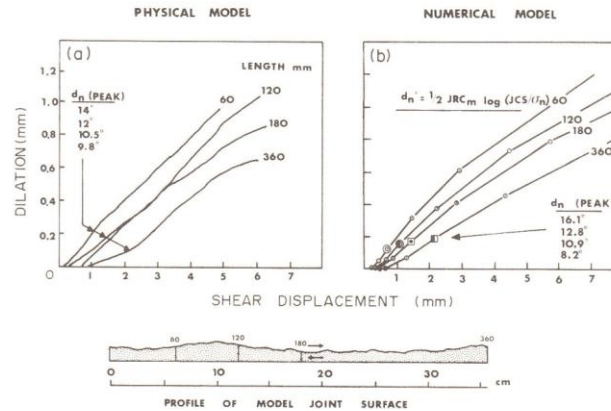


Fig. 18. Modelling the dilation-displacement data obtained from physical joint replicas of various sizes. Physical data was obtained from Bandis [4].

various sizes of shear box. Each of these samples was a portion of identical cast replicas of another rough bedding plane in limestone, whose roughness profile is shown in the figure.

Our numerical model was used to generate corresponding sets of dilation-displacement curves, using relevant input data obtained from the smallest physical models:

$$JRC_0 = 16.8, \quad JCS_0 = 2 \text{ MPa}, \quad \phi_r = 32^\circ.$$

The normal stress level applied in the physical model tests and in our numerical model was equivalent to full scale values of σ'_n and JCS_n of 2 and 80 MPa, respectively.

The comparison of physical and numerical data appears to be good. The somewhat variable curves seen in the physical data may be partly a function of the averaging process. The single 360 mm long sample gives a very similar 'S'-shaped curve to the numerical model.

PART IV—SHEAR CONDUCTIVITY COUPLING

Contact Areas in Matched and Mismatched Joints

When joints are fully interlocked (unsheared) there is a certain distribution of contact points whose total area (A_0) is generally a small percentage of the total sample area (A_1). The latter is the area used in converting applied loads to stress levels.

Experiments performed by Bandis [4] suggest that when shearing (mismatch) occurs the number of contact points may reduce, although individual areas may become larger. Bandis used a 12 μm polyester film inserted between the mating faces of joints to record the different distribution of contact points. Planar joints gave a uniform distribution of numerous small contact areas, while rough joints gave a non-uniform distribution of larger individual contact areas. Normal closure tests

conducted on joints representing five different rock types indicated ratios of A_0/A_1 in the range 0.4–0.7. The ratios of σ'_n/JCS applied in these tests generally ranged from 0.3 to 0.7, with a mean of 0.49 for the 12 tests reported in detail by Bandis [4].

In earlier work involving shear tests, reported by Barton and Choubey [7] it was observed that the ratio A_0/A_1 was related directly to the stress/strength ratio:

$$A_0/A_1 \approx \sigma'_n/JCS. \quad (17)$$

The estimates of A_0/A_1 were made from damaged areas measured in shear tests that were arrested after about 1 mm of shear when the peak strength of the joints had just been reached. By implication, contacting asperities are approximately reduced to compressive failure at the instant of peak strength.

Observation of contact areas made by Iwai [31] in normal closure (interlocked) tests on tension fractures in granite, provide some further support for the above model. Iwai's tests indicated ratios of A_0/A_1 of less than 0.001 when effective normal stress levels as low as 0.26 MPa were applied. At high stress levels (20 MPa) the ratio of A_0/A_1 was reportedly in the range 0.1–0.2. If we hypothesize a JCS value of approximately 200 MPa for the granite, the above ratios are approximately in accord with equation (17).

Dilation-Conductivity Coupling

The above data suggest that when water flow through a joint is considered, there will be similar total areas of asperity contact (blocked flow) whether the joint is under conditions of normal stress (interlocked) or shear (mismatched). If this assumption is valid, then the empirical relation between mechanical aperture (E) and conducting aperture (e) may also be applied to the phenomenon of dilation. The little available data lend support to this hypothesis.

Changes of mechanical aperture (ΔE) caused by dilation can be calculated from the tangent of the dilation

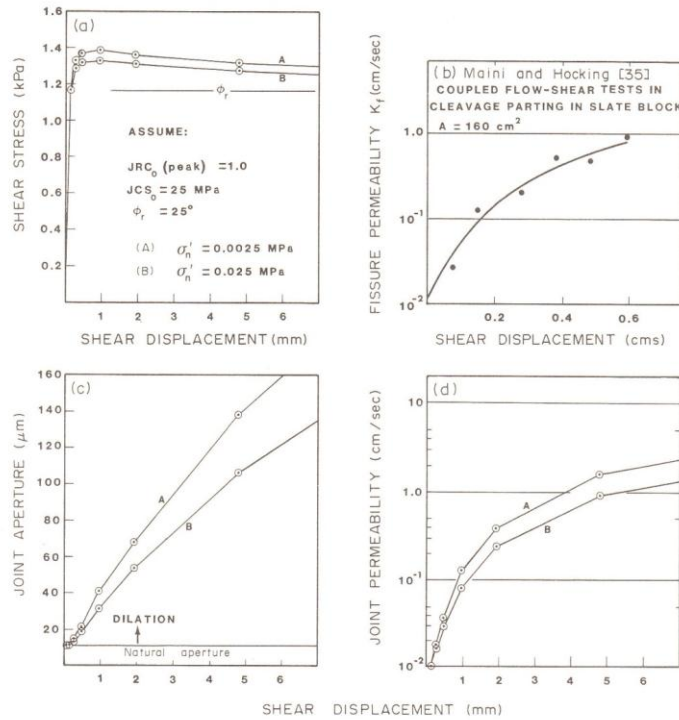


Fig. 19. Example of shear-dilation-conductivity modelling (diagrams a, c and d) and comparison with (b) experimental data from Maini and Hocking [35].

angle, since a given increment of shear displacement ($\Delta\delta$) will automatically result in a positive ΔE component. Thus for the general case:

$$\Delta E = \Delta\delta \cdot \tan d_n^*(\text{mob}). \quad (18)$$

The resulting values of ΔE are added to E and their sum converted to a conducting aperture (e) using the relation shown in Fig. 5. The resulting change of conductivity can be calculated from equation (5).

Comparison with measured data

Validation of the above coupling concept is necessarily limited due to the experimental difficulties of flow testing joints under conditions of shear. The measurements of dilation-induced changes in joint water pressure in a closed system is easier, but does not provide the necessary data.

At the time of writing the only data available for validation were those shown in Fig. 19. The tests were conducted by Maini [36] in a cleavage parting in a block of slate. The characterization data:

$$JRC_0 = 1.0, \quad JCS_0 = 25 \text{ MPa}, \quad \phi_r = 25^\circ,$$

are the author's estimates based on similar cleavage surfaces tested by Barton and Choubey [7].

The stress-displacement-dilation-conductivity modelling shown in Fig. 19 has been performed at two extremely low levels of effective normal stress to represent the self-weight loading used by Maini [36]. The initial aperture was derived from the initial conductivity. On the basis of the assumptions made, excellent agreement with the experimental data is indicated. Both the experiment and the model indicate the potential for at least two orders of magnitude change in conductivity with shear. Such effects will tend to be most marked for high values of JCS/σ'_n and high values of JRC , and will be more limited when stress levels are high, and when wall strength and roughness are low.

Examples of Shear-Dilation-Conductivity Coupling

In an earlier example of normal closure-conductivity coupling (Fig. 9) we subjected a medium rough ($JRC_0 = 10$), partly weathered ($JCS_0 = 75$ MPa, $\sigma_c = 150$ MPa) joint to four load-unload cycles, to obtain an approximation to *in situ* conditions. The initial conductivity of approximately 3×10^{-4} cm² under zero stress was thereby reduced to approximately 10^{-5} cm². Two stress levels (6 and 24 MPa) were selected from the fourth load cycle (circles, Fig. 9) to define initial conditions for potential shearing events. Shearing could be caused, for example, by the gradual increase in shear

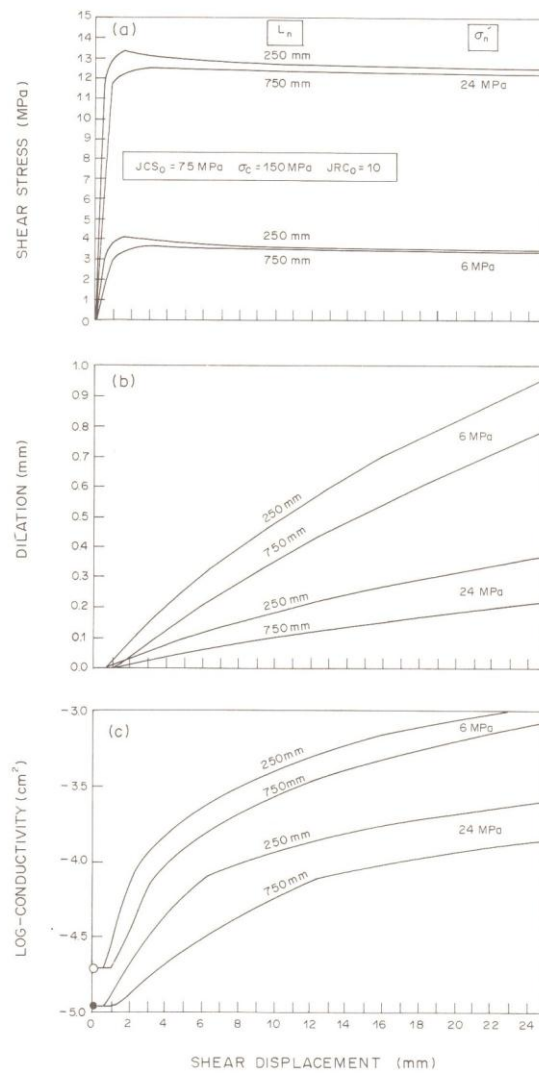


Fig. 20. Modelling potential shearing events for two *in situ* block sizes of 0.25 and 0.75 m, at constant effective normal stress levels of 6 and 24 MPa.

stress resulting from the near-field thermal pulse in a nuclear waste repository, or from tunnel excavation in a jointed medium. In some cases these processes would also result in increased normal stress. For the sake of simplicity, shearing under constant effective normal stress is assumed in these examples.

In Fig. 20, the shear–dilation–conductivity coupling is shown for two potential block sizes (or cross-joint spacings) of 0.25 and 0.75 m. These different sizes cause only minor differences in the shear–displacement behaviour, but quite marked differences in the magnitude of dilation and conductivity. Slightly delayed initiation of

dilation and conductivity is also seen, due to the change in block size.

A similar exercise to the above was performed with the normal closure–conductivity data described earlier for the joints in welded tuff. This modelling, which was performed for Sandia National Laboratories, is shown in Fig. 11. Points A, B and C on the fourth loading cycle are used as starting conditions for the shear–dilation–conductivity coupling shown in Fig. 21. Due to the relatively small size of blocks (0.1–0.25 m) there is a potential two orders of magnitude increase in conductivity for only 2 mm of shear, even when the effective

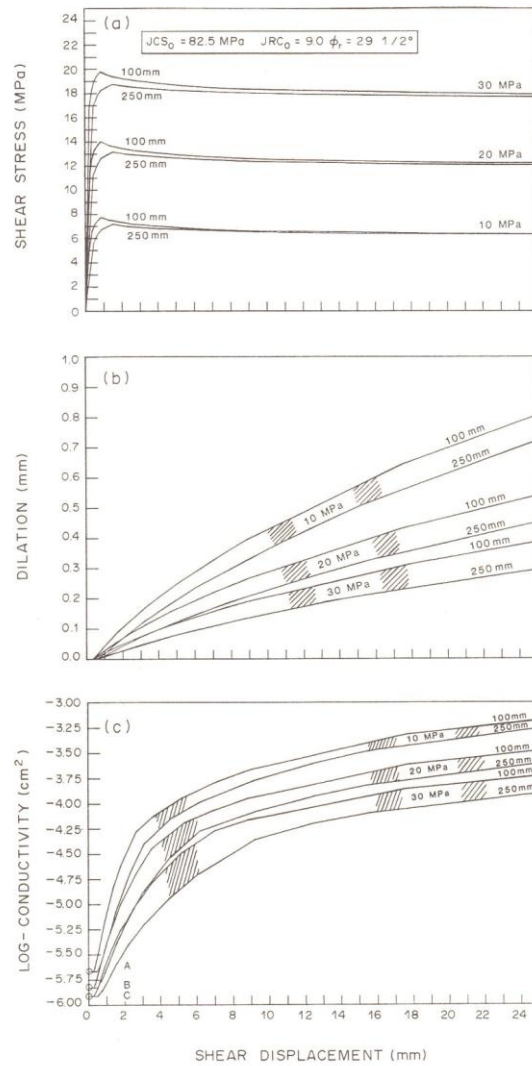


Fig. 21. Modelling the effect of potential shearing events for joints in welded tuff, following the normal closure modelling shown in Fig. 11.

normal stress is as high as 10 MPa. Such events would probably be rapidly inhibited underground, due to the plane strain type boundary conditions.

Further examples are given illustrating wider ranges of stress and block size to indicate the potential variations in behaviour. Figure 22 illustrates the potential effect of variations in effective normal stress, and Fig. 23 the potential effect of variations in block size. In both these examples, an initial conducting aperture (e) of $25 \mu\text{m}$ was assumed as representative of *in situ* conditions. This was the median value obtained from the borehole pumping tests performed in crystalline rock by Davison *et al.* [22].

Fully-Coupled, Hydrothermomechanical Joint Behaviour

The modelling capabilities illustrated in the foregoing discussion represent significant advances over previous joint modelling. Nevertheless, there is an important aspect that has been totally ignored, namely the effect of rock (and water) temperature. If sufficient testing had been performed, this aspect could have been addressed, but at present there is apparently only one set of published data. This is illustrated in Fig. 24.

The data were obtained from a flat-jack loaded block of jointed gneiss under conditions of normal stress with no shear component. The particular joint was sampled

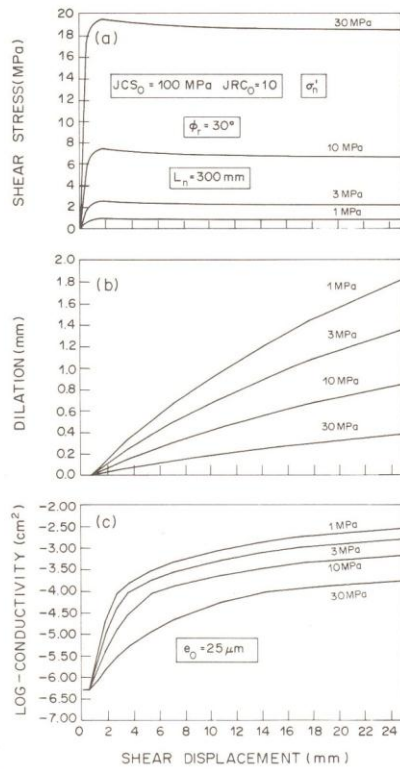


Fig. 22. Potential range of behaviour caused by shear under effective normal stress levels varying from 1 to 30 MPa.

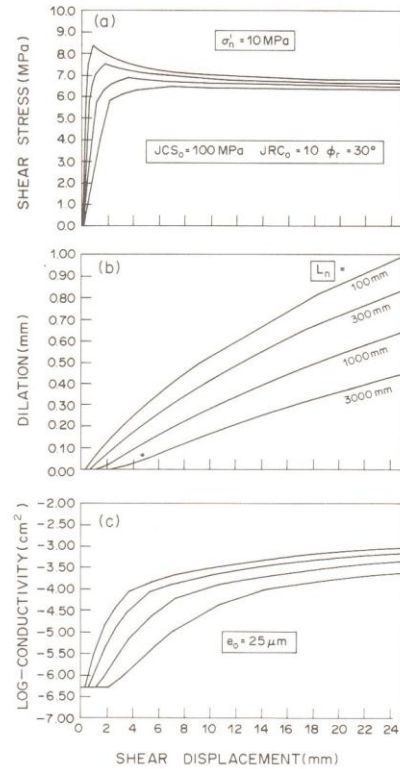


Fig. 23. Potential range of behaviour caused by shear of rock-masses with average block sizes ranging from 0.1 to 3.0 m.

by drill core, and was tilt tested as in Fig. 3. It was characterized as follows: $r = 39$, $R = 55$, $JCS_0 = 90$ MPa, $\sigma_c = 240$ MPa, $JRC_0 = 13$, $JRC_n = 7.9-8.3$ (for joint lengths L_n of 200–290 mm) $\phi_b = 31^\circ$, $\phi_i = 25^\circ$. The drill holes used for sampling the joint were subsequently used for water injection tests.

The area of joint actually loaded by the flat jacks exceeded 5 m^2 , but the flow test was conducted in an area of only about 0.08 m^2 , between parallel boreholes. The rock and water temperature in this zone is given along the diagonal axis in Fig. 24.

In summary, the test joint exhibited a four-fold reduction in conductivity when loaded from 0 to 6.9 MPa under ambient conditions, and a thirty-fold reduction when temperature was also increased to 74°C . Increased temperature alone, with no change in the normal stress, reduced the conductivity ten-fold.

The small conducting aperture ($9.1-16.1 \mu\text{m}$) was almost maintained by pressure alone during cooling, probably due to the high shear strength of the tightly mated walls. Significant 'lack of fit' did not occur until the aperture rebounded from 16.1 to $42.2 \mu\text{m}$, somewhere between the stress level of 3.45 and 0 MPa (points 20 and 21 in Fig. 24).

The above reduction of flow aperture with temperature was interpreted by Barton and Lingle [37] as improved mating of the opposed joint walls. The test joint was quite rough, and was undoubtedly formed at a temperature above the present 12°C , though how high is uncertain. A roughness profile of a joint measured at ambient temperature will not exactly match a profile measured while the joint is at elevated temperature, if thermal contraction is anisotropic. Elevated temperature and pressure probably partially recreated formation conditions.

The coupled closure-conductivity tests performed by Gale [32] illustrated that tighter apertures were achieved with artificial tension fractures than with natural joints in igneous rock. This is probably due to the fact that artificial tension fractures are generally formed at the same laboratory temperature at which they are flow tested, and their opposed faces therefore mate very tightly.

CONCLUSIONS

(1) The constitutive model of joint behaviour described in this paper provides realistic simulation of

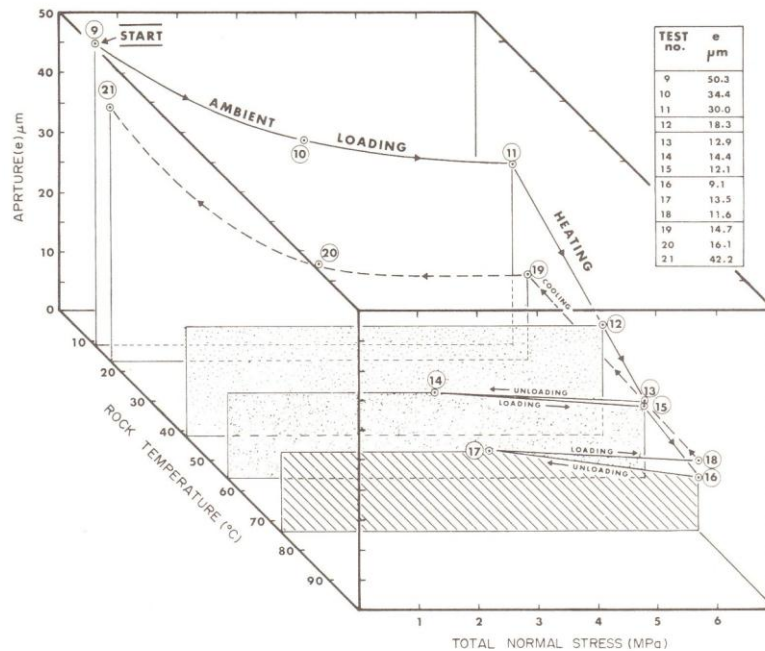


Fig. 24. Aperture-temperature-stress coupling for a rough, mineralized joint in gneiss. The data were obtained from an 8 m³ *in situ* heated block test, reported by Hardin *et al.* [23].

observed phenomena, and yet involves relatively inexpensive acquisition of joint data. Tilt tests and Schmidt rebound tests conducted on jointed core or on exposed jointed blocks are all that are required to obtain estimates of the roughness (JRC), the wall strength (JCS), the residual friction (ϕ_r) and the conducting aperture (e). Borehole pumping tests can be utilized if available.

(2) Unlike earlier constitutive models, the effect of test sample size and natural block size are specifically addressed, so that size effects can be modelled in a consistent manner. In general, increases in block size and in normal stress cause convergent behaviour between rock types. Small samples tested at low stress show divergent behaviour between rock types.

(3) The constitutive model provides shear stress-displacement-dilation-conductivity coupling and normal stress-closure-conductivity coupling. The shear-dilation modelling is based on the JRC (mobilized) concept, which represents the roughness mobilized or destroyed pre-peak or post-peak respectively. The normal closure modelling is based on a hyperbolic model for loading and unloading. The abscissae are characterized by initial normal stiffness (K_{ni}) and maximum closure (V_m), both of which are dependent on roughness (JRC) and wall strength (JCS).

(4) In general, smooth joints in weak rocks close most readily under normal stress, and display low shear strength and weak coupling between shearing and conductivity. Conversely, rough joints in strong rocks close

least under normal stress, and display high shear strength and strong coupling between shearing and conductivity.

(5) An important aspect of the coupling between joint deformation and conductivity, is the mismatch of the mechanical aperture (E) and the theoretical smooth wall conducting aperture (e) used in the cubic law for flow rate. Areas of asperity contact, tortuous flow, and wall roughness account for these differences, which can now be quantified, based on a constitutive model relating, E , e and JRC.

(6) The joint modelling concepts developed in this paper have been utilized in several engineering design problems, of which the following is a summary: rock slope stability, rock bolt reinforcement of adversely dipping joints, three-dimensional wedge stability in an arch dam abutment, grout-take calculations in a permeable dam foundation, leakage along major joints into a tunnel, near-field modelling of conductivity variations in planned nuclear waste repositories, chip resistance in sub-sea dredging operations in soft rocks, modelling dilation and stress-path effects under static and dynamic loading.

(7) Future application in other areas such as petroleum reservoir technology and geothermal projects appears warranted. For example, waterflood treatments to improve oil and gas production involve fundamental effective stress-closure-conductivity coupling mechanisms which can now be modelled. Similarly, hydrofrac

treatments in an anisotropic stress environment in which jointing does not parallel the principal stress, may also stimulate fundamental shear-dilation-conductivity coupling mechanisms. These events can be modelled if the joints are characterized and if the existing total and effective stresses are known.

Acknowledgements—The work described in this paper was supported by the following institutions: the Norwegian Geotechnical Institute and NTNf in Oslo, the Earth Science Department in the University of Leeds, the Office of Nuclear Waste Isolation in Columbus, Ohio, the CANMET Mining Research Laboratories in Ottawa and Sandia National Laboratories in Albuquerque, New Mexico. This support, and the hard work and enthusiasm of Vishnu Choubey, Ernest Hardin, Alistair Lumsden and Alfred Annor are gratefully acknowledged.

Received 20 August 1984.

REFERENCES

- Link H. The sliding stability of dams. *Water Pwr* March, April, May, Parts I, II and III (1969).
- Goodman R. E. Deformability of joints. *Symp. Determination of the In situ Modulus of Deformation of Rock*, American Society for Testing Materials, STP 477, pp. 174–196 (1970).
- Cundall P., Marti J., Beresford J., Last P. and Asagian M. Computer modeling of jointed rock-masses. Rept by Dames and Moore, London, for U.S. Army Engineer Waterways Experiment Station, Vicksburg, 396 pp. (1978).
- Bandis S. Experimental studies of scale effects on shear strength and deformation of rock joints. Ph.D. thesis, Univ. of Leeds, Dept of Earth Sciences (1980).
- Barton N. and Bakhtar K. Rock joint description and modelling for the hydrothermomechanical design of nuclear waste repositories. Contract Rept. Submitted to CANMET, Mining Research Laboratories, Ottawa. Parts 1–4, 270 pp. Part 5, 108 pp. (1983).
- Pratt H. R., Black A. D. and Brace W. F. Friction and deformation of jointed quartz diorite. *Proc. 3rd Int. Congr. on Rock Mechanics*, Denver, Colorado, Vol. 2A, pp. 306–310 (1974).
- Barton N. and Choubey V. The shear strength of rock joints in theory and practice. *Rock Mech.* **10**, 1–54. (1977).
- Bandis S., Lumsden A. C. and Barton N. Experimental studies of scale effects on the shear behaviour of rock joints. *Int. J. Rock Mech. Min. Sci. & Geomech. Abstr.* **18**, 1–21 (1981).
- Barton N. and Bandis S. Effects of block size on the shear behaviour of jointed rock. Keynote Lecture, *23rd U.S. Symp. on Rock Mechanics*, Berkeley, California (1982).
- Barton N. The shear strength of rock and rock joints. *Int. J. Rock Mech. Min. Sci. & Geomech. Abstr.* **13**, 255–279 (1976).
- Byerlee J. D. Friction in rocks. *J. Pure Appl. Geophys.* **116**, 615–626 (1978).
- Bandis S., Lumsden A. C. and Barton N. Fundamentals of rock joint deformation. *Int. J. Rock Mech. Min. Sci. & Geomech. Abstr.* **20**, 249–268 (1983).
- Rocha M. Mechanical behaviour of rock foundations in concrete dams. *Trans. Int. Congr. on Large Dams*, Vol. 8, Vol. 1, pp. 785–831. Edinburgh (1964).
- Cramer M. L., Cunningham J. P. and Kim K. Rock mass deformation properties from a large-scale block test. *Bull. Am. Engng Coun.* **XXI**, 47–54 (1984).
- Coulomb C. A. Essai sur une application des règles de maximis et minimis à quelque problèmes de statique relatifs à l'architecture. *Mém. Math. Phys. Acad. R. Sci., Paris* **5(7)**, 343–382 (1773). (Published in 1776).
- Jaeger J. C. The frictional properties of joints in rock. *Geofis. pura appl.* **43**, 148–158 (1959).
- Patton F. D. Multiple modes of shear failure in rock and related materials, p. 282. Ph.D. thesis, Univ. of Illinois (1966).
- Rengers N. Unebenheit und Reibungswiderstand von Gesteinstrennflächen (Roughness and friction properties of separation planes in rock). Thesis, Technische Hochschule Friederician, Karlsruhe, Institut für Bodenmechanik und Felsmechanik Veröffentlichungen **47**, 129 (1971).
- Barton N. A relationship between joint roughness and joint shear strength. *Rock Fracture—Proc. Int. Symp. on Rock Mechanics*, Nancy, France, Paper 1–8 (1971).
- Miller R. P. Engineering classification and index properties for intact rock, p. 332. Ph.D. thesis, Univ. of Illinois (1965).
- Snow D. T. Rock fracture spacings, openings and porosities. *Proc. Am. Soc. civ. Engrs* **96 (SM 1)**, 73–91 (1968).
- Davison C. C., Keys W. S. and Paillet F. L. Use of borehole-geophysical logs and hydrologic tests to characterize crystalline rock for nuclear-waste storage. ONWI-418, 103 pp. (1982).
- Hardin E. L., Barton N., Lingle R., Board M. P. and Voegelé M. D. A heated flatjack test series to measure the thermo-mechanical and transport properties of *in situ* rock masses. Office of Nuclear Waste Isolation, Columbus, Ohio, ONWI-260, 193 pp. (1982).
- Witherspoon P. A., Wang J. S. Y., Iwai K. and Gale J. E. Validity of cubic law for fluid flow in a deformable rock fracture. Lawrence Berkeley Laboratory, LBL-9557, SAC-23, 28 pp. (1979).
- Sharp J. C. Fluid flow through fissured media. Ph.D. thesis, Univ. of London (1970).
- Danielsen S. W. Joint permeability. Thesis (in Norwegian), Norwegian Technical Univ., Trondheim (1971).
- Heimli P. Water and air leakage through joints in rock specimens (in Norwegian). *Fjellsprengningsteknikk, Bergmekanikk, Annual Rock Mechanics Meeting*, Oslo, Norway, pp. 137–142 (1972).
- Kranz R. L., Frankel A. D., Engelder T. and Scholz C. H. The permeability of whole and jointed Barre granite. *Int. J. Rock Mech. Min. Sci. & Geomech. Abstr.* **16**, 225–234 (1979); Erratum, **17**, 237–238 (1980).
- Schrauf T. W. Relationship between the gas conductivity and geometry of a natural fracture. M.Sc. thesis, Dept of Hydrology and Water Resources, Univ. of Arizona, 156 pp. (1984).
- Barton N. Modelling rock joint behaviour from *in situ* block tests: implications for nuclear waste repository design. Office of Nuclear Waste Isolation, Columbus, Ohio, ONWI-308, p. 96 (1982).
- Iwai K. Fundamental studies of fluid flow through a single fracture. Ph.D. thesis, Univ. of California, Berkeley, 208 pp. (1976).
- Gale J. E. The effects of fracture type (induced versus natural) on the stress-fracture closure-fracture permeability relationships. *Proc. 23rd U.S. Symp. on Rock Mechanics*, Univ. of California, Berkeley, pp. 290–298 (1982).
- Kulhawy F. H. Stress-deformation properties of rock and rock discontinuities. *Engng Geol.* **9**, 327–350.
- Hungro O. and Coates D. F. Deformability of rock joints and its relation to rock foundation settlements. *Can. Geotech. J.* **15**, 238–249 (1978).
- Maini T. and Hocking G. An examination of the feasibility of hydrologic isolation of a high level repository in crystalline rock. *Geologic Disposal of High-Level Radioactive Waste Session, Annual Meeting of the Geological Society of America*, Seattle, Washington, (1977).
- Maini T. *In-situ* hydraulic parameters in jointed rock, their measurement and interpretation. Ph.D. thesis, Imperial College, London, 312 pp. (1977).
- Barton N. and Lingle R. Rock mass characterization methods for nuclear waste repositories in jointed rock. *ISRM Symp. on Rock Mechanics, Caverns and Pressure Shafts*, Aachen, Balkema, Rotterdam (1982).